Computers in Biology and Medicine 107 (2019) 265–269

Contents lists available at ScienceDirect

Computers in Biology and Medicine

journal homepage: www.elsevier.com/locate/compbiomed

Muscle fibre morphology and microarchitecture in cerebral palsy patients obtained by 3D synchrotron X-ray computed tomography

Leise Borg[a,*], Jon Sporring[a], Erik B. Dam[a], Vedrana A. Dahl[b], Tim B. Dyrby[b,c], Robert Feidenhans'l[d], Anders B. Dahl[b], Jessica Pingel[e]

[a] Department of Computer Science, University of Copenhagen, Denmark
[b] Department of Applied Mathematics and Computer Science, Technical University of Denmark, Kongens Lyngby, Denmark
[c] Danish Research Centre for Magnetic Resonance, Center for Functional and Diagnostic Imaging and Research, Copenhagen University Hospital Hvidovre, Hvidovre, Denmark
[d] European XFEL, Schenefeld, Germany
[e] Department of Neuroscience, University of Copenhagen, Denmark

ARTICLE INFO

Keywords:
Cerebral palsy
Muscle
Morphology
Synchrotron computed tomography
Three-dimensional images
Orientation consistency

ABSTRACT

Background: Synchrotron X-ray computed tomography (SXCT) allows for three-dimensional imaging of objects at a very high resolution and in large field-of-view.
Purpose: The aim of this study was to use SXCT imaging for morphological analysis of muscle tissue, in order to investigate whether the analysis reveals complementary information to two-dimensional microscopy.
Methods: Three-dimensional SXCT images of muscle biopsies were taken from participants with cerebral palsy and from healthy controls. We designed morphological measures from the two-dimensional slices and three-dimensional volumes of the images and measured the muscle fibre organization, which we term orientation consistency.
Results: The muscle fibre cross-sectional areas were significantly larger in healthy participants than in participants with cerebral palsy when carrying out the analysis in three dimensions. However, a similar analysis carried out in two dimensions revealed no patient group difference. The present study also showed that three-dimensional orientation consistency was significantly larger for healthy participants than for participants with cerebral palsy.
Conclusion: Individuals with CP have smaller muscle fibres than healthy control individuals. We argue that morphometric measures of muscle fibres in two dimensions are generally trustworthy only if the fibres extend perpendicularly to the slice plane, and otherwise three-dimensional aspects should be considered. In addition, the muscle tissue of individuals with CP showed a decreased level of orientation consistency when compared to healthy control tissue. We suggest that the observed disorganization of the tissue may be induced by atrophy caused by physical inactivity and insufficient neural activation.

1. Introduction

Cerebral Palsy is considered a neurological disorder caused by a non-progressive brain injury that occurs either before, during or shortly after birth [1]. Cerebral Palsy primarily affects body movement and posture, but cognitive malfunctions are also common [2]. As a secondary response to the brain injury, individuals with cerebral palsy experience various muscular symptoms including muscle weakness [3], impaired muscle growth [4], spasticity [5] and increased passive stiffness [6]. Increased muscle stiffness, also called muscle contractures is, however, the most limiting factor that influences individuals with CP since it hinders normal movement [7]. The mechanisms that lead to the development of contractures are still poorly understood. Proper description and characterization of contractures as a muscle-phenotype might be able to reveal some of the mechanisms behind contracture development.

Muscle biopsies play an integral role in the evaluation of patients with neuromuscular diseases. Morphologic analyses are used in research settings for cerebral palsy, and common pathologic findings include a decrease in fibre size and an increase in fibre size variation. The evaluations are often carried out on two dimensions (2D) histochemical images or other image modalities in 2D. For 2D analysis of muscle

* Corresponding author.
E-mail address: leiseborg@gmail.com (L. Borg).

https://doi.org/10.1016/j.compbiomed.2019.02.008
Received 24 August 2018; Received in revised form 13 February 2019; Accepted 13 February 2019
0010-4825/

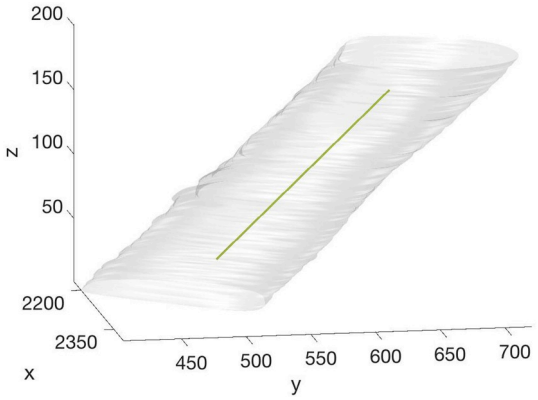

Fig. 1. A segmentation of a muscle fibre, which is not aligned with the scanning slices in the 3D volume. Therefore, 2D slice-by-slice analysis is not performed perpendicular to the fibre orientation; as a consequence, the cross-sectional area is overestimated, with an average of 1370 μm^2 (see the 2D morphology Section). The green line visualizes the fibre orientation as determined by the 3D analysis we propose (see the 3D morphology Section). When estimating the cross-sectional area perpendicular to the orientation, the cross-sectional area was estimated to be 980 μm^2.

fibres, there exist several automatic and semi-automatic segmentation methods [8,9], some of which are based on active contours [10–12] whereas others combine threshold selection and morphology techniques [13,14]. The use of three-dimensional (3D) SXCT images is a new alternative to 2D histochemical-based images as we recently have presented [15–17].

For reliable morphological results, the biopsy must be orientated such that muscle fibres extend perpendicularly to the slice plane [18]. However, it may occur that the biopsy has been tilted during tissue preparation or the samples have low orientation consistency, i.e., the muscle fibres are not organized parallel and point in different directions. Then, a subsequent morphologic analysis will be prone to errors because those fibres not extending perpendicularly to the slice plane appear with higher cross-sectional areas and altered shapes. Fig. 1 illustrates a segmented fibre from one of the scanned biopsies that is tilted with respect to the orientation of the scan. Straightforward 2D slice-wise analysis of this 3D scan resembles the analysis that is possible when performing microscopy on actual biopsy slices (after cutting). The 2D slice-wise analysis leads to a large over-estimation of the cross-sectional area – because the slices are not perpendicular to the fibre orientation. Specifically, the estimated mean cross-sectional area is 1370 μm^2 from the 2D analysis and 980 μm^2 from the 3D analysis (please, see the sections 2D morphology and 3D morphology for details).

Imaging the microstructure of tissue in 3D at a resolution similar to optical microscopy used in histopathology has become possible with the development of large-scale synchrotron X-ray imaging facilities [19]. Synchrotron X-ray computed tomography (SXCT) allows for 3D imaging of objects at a very high resolution and very large field-of-view (FOV). The high photon flux, monochromatic, tuneable beams in synchrotrons together with methods like phase contrast allows for contrast in tissue despite little difference attenuation, and therefore permit non-destructive ex-vivo examination of various specimens in various depths and at different scales [20,21]. X-ray computed tomography is most widely used in clinical practice for in-vivo examination, but the use of SXCT for bio-imaging is at a resolution that is comparable to optical microscopy, is non-destructive to the tissue (no physical slicing) and provides an isotropic image resolution, but still the EM typically has higher in-plane image resolution [22].

The sample size and radiation dose will most often only allow for ex-vivo investigations, but the technique is very well suited for studying muscle fibre biopsies as done here. 3D structures of single muscle fibres on a sub-micrometre scale were clearly visible, but it did not reveal substructures such as myofibrils.

In the present study, images were acquired at the Swiss Light Source (SLS) at the TOMCAT beamline that allows for volumetric X-ray CT imaging at sub-micrometre resolution. Our aim was to make a 3D analysis of muscle fibres and to test whether a 3D analysis should be considered in place of the classical 2D analysis for fibre morphology. We hypothesised that the muscle fibre cross-sectional areas from participants with cerebral palsy were smaller than those from healthy participants. This is demonstrated on tissue biopsies from people with cerebral palsy (CP) and healthy controls (H) in a study with a total of 30 participants.

2. Materials and methods

2.1. Subjects

A total of 30 muscle biopsies were taken: 20 biopsies from participants with cerebral palsy and 10 from healthy participants. The muscle biopsies were obtained from the medial Gastrocnemius muscle after local anesthesia (1% lidocaine) and incision of the overlying skin. The biopsy was taken using a 5-mm Bergstrom needle (Stille, Stockholm, Sweden) with manual suction. The obtained muscle biopsies weighted around 80–100 mg.

The local ethical committee has approved the procedure with protocol number H-2-2014-028.

2.2. Sample preparation

The biopsies were embedded in Bouin's fluid and stored at 4° Celsius for 48 h. After that, the biopsies were washed with 98% Ethanol for 5 min six times. Subsequently, the biopsies were stored in 98% EtOH at 4° Celsius until analysis.

2.3. Acquisition

Imaging was done at the TOMCAT beamline at the Swiss Light Source using synchrotron X-ray CT. Only the central part of the biopsy was imaged, resulting in an image of 2560 × 2560 × 2160 voxels. This 3D image can also be viewed as 2160 virtual 2D slices with resolution 2560 × 2560, stacked on top of each other. The voxel size is $(330\,nm)^3$, so the depicted volume is 844 × 844 × 773 μm^3. 1500 projections covering 180° were obtained, and a filtered back-projection based algorithm was used for tomographic reconstruction. For details of image acquisition, please refer to Ref. [15]. Fig. 2 shows a slice example from each of the two groups. Visual inspection revealed that the image quality is much lower in the periphery of the sample because X-rays did not traverse these parts of the sample from all angle projections in the SXCT-scan. Therefore, to ensure robust segmentation and analysis, the

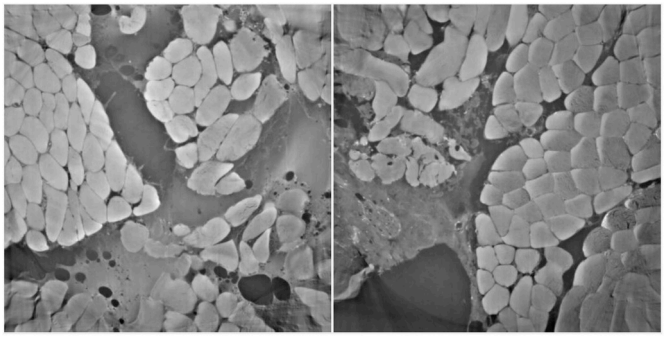

Fig. 2. Example of slice number 1000 from one member of both groups. The left image shows muscle tissue from an individual with CP, and the right image shows muscle tissue from a healthy individual.

corners of the images are left out when analysing the images.

2.4. Muscle fibre segmentation

A fully automated segmentation of muscle fibres is challenging, mainly because of the great variations in the images. Therefore, we used a semi-automated method based on a 2D snake [23]. The 2D snake was initialized as a circle in a (virtual) 2D slice, and the image was unfolded by sampling along the normal vectors to the snake. In the unfolded image, the position of the fibre boundary was found using a graph-cut approach of [24] which was set up such that snake is attracted by the big change in the intensity, which characterizes fibre boundary. The segmentation was constrained by limiting curves normal displacement, to ensure smoothness of the segmentation. The segmentations from one slice were passed on to the following slice and used as offsets to the subsequent segmentations. For every 20 slices, the segmentations were semi-automatically adjusted and new snakes were initialized if new fibres had entered the image.

Here we analysed only a sub-volume including 201 slices (from slice 100 to 300) that resulted in a 3D image volume being 66 μm in height and of 844 μm in diameter. We limited the number of slices to limit the workload in the interactive segmentation – while making sure the slice range was easily sufficient to allow the intended analysis: to find cross-section areas and orientations of the fibres. Fig. 3 shows examples of a volumetric segmentation in 3D from one member of both groups.

2.5. 2D morphology

In each slice, the cross-sectional areas of individual fibres were calculated based on the average in 201 slices. The number of pixels belonging to each fibre was calculated and multiplied with the image resolution of $(0.33\,\mu m)^2$/pixel. The overall orientation of the fibres is perpendicular to the slices, however, is not necessarily the case for every single fibre. Therefore, the cross-sectional areas of those fibres not extending exactly perpendicularly to the image plane are biased towards higher values.

2.6. 3D morphology

The 3D segmentations were presented as surface renderings of the segmentations in the 201 slices. 3D surface normal vectors were computed from the segmented muscle fibres in each node of the segmented surface. To calculate the cross-sectional areas, we virtually sliced each muscle fibre orthogonal to the overall fibre direction. Fibre direction was identified by analysing its surface normal vectors, N_k; The outer product of the set of normals was summarized to obtain the matrix, M, known as the Structure Tensor [25]. In this case, it is a 3×3 matrix. For a perfectly straight fibre, most of its normals will be perpendicular to the fibre's direction, and the two eigenvectors of M corresponding to the two largest eigenvalues in absolute sense span the cross section of the fibre, and the eigenvector, d, corresponding to the smallest eigenvalue is parallel to the overall direction of the fibre. With the fibre directions at hand, we estimated the cross-sectional area as follows:

Fig. 3. Example of a volumetric segmentation in 3D from one member of both groups. The left image is from an individual with CP, and the right image is from a healthy individual.

1. Project  the points $P(l)$ of the segmentation from the fibres's surface onto the plane perpendicular to d, to obtain the residuals points, $R(l)$: $R(l) = P(l) - (P(l)\cdot d)d$.
2. Make a principal component analysis on the cloud of residual points, $R(l)$, to obtain the principal component variances a and b in the plane perpendicular to d. The standard deviations are $\sqrt{a}$ and $\sqrt{b}$.
3. Assume the cross-section is approximately elliptical and estimate the area of the cross-section as the area of an ellipse with $\sqrt{a}\sqrt{2}$ and $\sqrt{b}\sqrt{2}$ as the lengths of its main axes: $A = 2\pi\sqrt{ab}$.

2.7. Orientation consistency

We developed an algorithm to quantify the fibre orientation consistency, i.e., the muscle fibres organization with respect to their orientations. We used the entropy of the fibre orientation distribution for each sample to estimate the orientation consistency as follows: All fibre orientations were represented by two vectors, d and $-d$ and plotted on a sphere. A 2D histogram for the azimuth-elevation coordinates with 12 bins in each angular direction was evaluated by estimating the entropy. Comparing the true entropy on the unit sphere from a uniform distribution with 1000 random samples drawn from a uniform distribution tested the method, and the error was less than 2.1%. For further details, please refer to Ref. [26].

2.8. Statistical analysis

The mean cross-sectional area for each individual, A_{ind}, was calculated for the 2D morphology and the 3D morphology by adding the individual fibre cross-sectional area in each individual and dividing by the number of total fibres in that individual. The standard deviations (STD) were calculated as:

$$STD = \sqrt{\frac{\sum |A_{ind} - \bar{A}_{ind}|^2}{n}},$$

where $\bar{A}_{ind}$ is the average of the cross-sectional area of all participants and n is the number of participants in each group.

The SEM was calculated as:

$$SEM = \frac{STD}{\sqrt{n}}.$$

To test for significant differences between the measures for the healthy participants and the participants with cerebral palsy, we used Matlab's (version R2017a) implementation of a two-sample t-test, “ttest2”. It returns a significance level, which is the p-value.

3. Results

Estimation of orientations: Fig. 4 shows one example of the calculated fibre orientations in each group. The orientations are represented by lines, which all have the same length regardless of the size of the fibre.

Cross-sectional area: The 2D analysis of the cross-sectional areas showed that muscle fibres of the CP group had a mean cross-sectional area of 6000 ± 5000 μm^2 (Mean ± STD) while the muscle fibres of the H group had a mean cross-sectional area of 7400 ± 4700 μm^2 (Fig. 5). The 3D analysis revealed that the muscle fibre cross-sectional area of the CP group was only 2600 ± 2400 μm^2 while the H group showed a cross-sectional area of 4500 ± 2900 μm^2 (Fig. 5). Evaluations using a two-sample t-test showed that the CP group had a significantly smaller muscle fibre cross-sectional area when compared to the healthy control group (H) using 3D analysis of the muscle fibres ($p < 0.0004$) (Table 1).

Orientation consistency: The entropy analysis showed that the

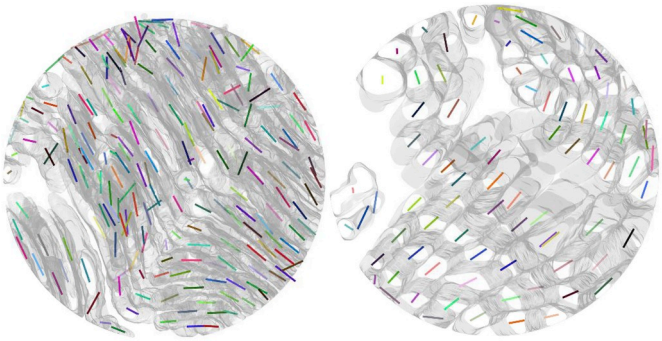

Fig. 4. Example of the fibre organization analysis (from the entropy analysis) from one member of both groups. The left image shows an individual with CP, and the right image shows a healthy individual.

mean orientation consistency between the two groups was significantly different ($p < 0.04$) (Fig. 5 and Table 1). While the CP group had an entropy index of 1.04 nits (nits = natural units of information), the H group has an entropy of 0.58 nits (Table 1).

4. Discussion

The major finding of the present study was that the 2D cross-sectional areas of the muscle fibres in the CP group were almost indistinguishable from the H group (p-value of 0.5). However, when analysing the data in 3D, the mean cross-sectional area was significantly larger for H than for CP ($p < 0.0004$). This observation is in line with previous studies showing that individuals with CP have smaller muscles when compared to typically developed individuals [27,28]. Ultrasound studies have shown that the muscles of individuals with CP have a significantly smaller muscle volume. Another study has shown that muscle thickness is significantly related to the motor function in adults with CP [29]. Even though it has been shown consistently that individuals with CP have smaller muscles it is not fully understood as to why the muscles are smaller.

Several studies have shown that individuals with CP are more inactive than typically developed individuals [30,31]. Furthermore, the ability to walk is clearly associated with physical activity levels [32]. Maltais et al. observed that individuals with CP that could walk had higher odds of being physically active and that the severity of their condition was associated with inactivity. At the same time, they observed that the inactivity levels in non-walkers were related to limitations of the range of motion during movement [32]. In addition, one study showed that older age and reduced community participation was associated with inactivity in individuals with cerebral palsy [33]. A lack of physical activity might partly explain why the muscles of individuals with CP are smaller.

However, besides inactivity, some authors have suggested that decreased muscle growth may cause smaller muscles in individuals with CP [34]. It has been shown that muscle growth in children with CP initially follows that of typically developing children, but decreases at 15 months of age [4]. Furthermore, the decreased rate of muscle growth is accompanied by an increase in passive muscle stiffness [35]. The present finding of smaller muscle fibres in the CP group does not as such explain whether the fibres are smaller due to lack of growth or atrophy. Nevertheless, the present findings reveal that the muscle tissue of the CP group had a significantly lower mean orientation consistency when compared to the control group, which indicates, that the microstructure of the muscle tissue of the individuals with CP is more disorganized than that of healthy control individuals. This observation has also been made in a previous study investigating the effect of BoNT injections on the micro-architecture of the muscle in rats [15]. In this study by Pingel et al. the disorganization of the tissue was a clear indicator of muscle atrophy following BoNT injections [15]. This leads us to suggest, that muscle atrophy might be partly responsible for the smaller muscle fibres and tissue disorganization that have been measured in the present study in adults with CP, and further that the muscle atrophy may be related to reduced physical activity and reduced neural activation of the muscle.

Table 1
Cross-sectional areas in 2D and 3D: means and standard deviations.

	Mean cross-sectional areas		STD of cross-sectional area		Entropy
	2D	3D	2D	3D	3D
CP	6300	2300	5000	1700	1.04
H	7400	3900	4700	2000	0.58
p-value	0.5	0.0004	0.9	0.4	0.04

The table shows the mean cross-sectional areas in 2D and 3D in μm^2, the mean STD of the cross-sectional areas in 2D and 3D and the fibre orientation (entropy) in natural units of information (nits). The significances for CP and H are estimated by the p-values in the bottom row.

In the present work, we focused 3D analysis of muscle fibres on a µm scale, which, to our knowledge, has not been done before.

While the methods and analysis were applied to muscle fibres, the same principles are applicable to other types of fibrous materials and on other scales, such as nerve fibres or carbon fibres.

Possible extensions of the 3D analysis include more morphological measures such as roundness, a skeletonisation of the segmentation and staining the samples to highlight specific types of tissue, such as fibre type or cell nuclei. We leave such investigations for future work.

One major limitation of the present study was that we only segmented 201 slices from each of our 30 samples. In tissues with very varying components, an analysis of one sub-volume only might cause inaccurate results. However, the number of fibres and samples analysed in the present study should mount to a reasonable dataset size, and should, therefore, average out any intra-tissue differences.

Another limitation of the present analysis was that we carried out analysis on all available segmentations of the chosen sub-volume of the samples - also fibres touching the edges of the region of interest. Some

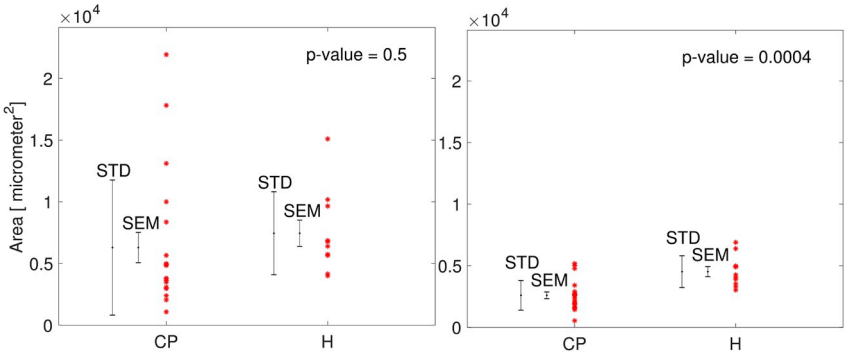

Fig. 5. Cross-sectional areas are shown for participants with CP and healthy participants. The left image shows the cross-sectional areas calculated from the 2D slices not taking into account that some fibres do not extend perpendicularly to the image plane. The right image (b) shows the cross-sectional areas calculated from the 3D volumes by the use of each muscle fibre direction. The bars left of the measurements in both images show the STD and SEM. The p-values in the top right corners denote the significance of the cross-sectional areas when comparing the two groups. The plots show that there is a much tighter spread in cross-sectional areas and a lower p-value when the analysis is conducted in 3D.

samples contained almost only fibres extending in the slice planes, almost all of them touching the edges of the image. These segmentations were kept in order to keep as much information as possible. The consequence was probably smaller cross-sectional areas in general across all samples and in both 2D and 3D measures. As only a small fraction of the total amount of fibres touched the edges, we anticipate that the measures are still robust.

In addition, the cross-sectional areas based on the Structure Tensor's estimate of the main fibre directions were overestimated in rare cases, whenever a fibre is not straight. However, for the vast majority of the fibres, the method seemed to capture the areas well, and as the numbers of incorrect fibre orientation estimates were very low, we considered the morphology measures to be rather reliable. The Structure Tensor analysis could have allowed the fibre direction to vary along its extension by splitting the analysis into separate parts of the fibre. However, we considered the present method to be a decent first approach, which showed the expected differences in the cross-sectional areas between the two groups.

Obtaining the cross-sections from the 3D volumes, an elliptic shape of the cloud of residual vectors was anticipated, which is not strictly correct for all fibres, but yet a sensible approximation. Because there were no outliers in the 3D cross-section areas (see Fig. 5), we are convinced that measurements carried out on fibres were usable.

5. Conclusion

The present study demonstrated that individuals with CP had smaller muscle fibres when the morphology of muscle biopsies was analysed using 3D volumes on SXCT images. When the same analysis was carried out on 2D slices no differences were observed indicating that the fibre orientation and positioning of muscle samples when analysing slices is of crucial importance for the results. Furthermore, the CP group had a significantly lower orientation consistency when compared to the control group indicating that the muscle tissue of the individuals with CP was more disorganized than the control tissue. The disorganization of the tissue may be caused by muscle atrophy, which might be induced by a lack of physical activity and insufficient neural activation of the muscle.

Our study demonstrated that it indeed is possible to use SXCT imaging for morphological analysis of muscle tissue and that the image resolution is similar to 2D microscopy but in full 3D. With further developments in SXCT techniques, this has great promise of morphological analysis of tissue in the future.

Conflicts of interest

None declared.

Acknowledgements

TD was supported by the Capital Region Research Foundation (Grant number: A5657) on the MAX4Imagers project. JP was supported by the Danish Research Council (DFF-1333-00197), DANSCATT and the Elsass Foundation.

References

[1] A. Colver, C. Fairhurst, P.O. Pharoah, Cerebral palsy, Lancet 383 (9924) (2014) 1240–1249.
[2] H.K. Graham, et al., Cerebral palsy, Nat. Rev. Dis. Primers 2 (2016) 15082.
[3] L. Barber, R. Barrett, G. Lichtwark, Medial gastrocnemius muscle fascicle active torque-length and Achilles tendon properties in young adults with spastic cerebral palsy, J. Biomech. 45 (15) (2012) 2526–2530.
[4] A. Herskind, et al., Muscle growth is reduced in 15-month-old children with cerebral palsy, Dev. Med. Child Neurol. 58 (5) (2016) 485–491.
[5] P. Crenna, Spasticity and 'spastic' gait in children with cerebral palsy, Neurosci. Biobehav. Rev. 22 (4) (1998) 571–578.
[6] S.S. Geertsen, et al., Impaired gait function in adults with cerebral palsy is associated with reduced rapid force generation and increased passive stiffness, Clin. Neurophysiol. 126 (12) (2015) 2320–2329.
[7] K.P. Murphy, The adult with cerebral palsy, Orthop. Clin. N. Am. 41 (4) (2010) 595–605.
[8] J. Mula, et al., Automated image analysis of skeletal muscle fiber cross-sectional area, J. Appl. Physiol. 114 (1) (1985) 148–155 2013.
[9] P.M.C. Poggi, R. Scelsi, Automatic morphometric analysis of skeletal muscle fibers in the aging man, Anat. Rec. (217) (1987) 30–34.
[10] F. Liu, et al., Automated fiber-type-specific cross-sectional area assessment and myonuclei counting in skeletal muscle, J. Appl. Physiol. 115 (11) (1985) 1714–1724 2013.
[11] Y.J. Kim, et al., Fully automated segmentation and morphometrical analysis of muscle fiber images, Cytometry 71 (1) (2007) 8–15.
[12] O.K.H. Röhrle, M. Loch, Segmentation of Skeletal Muscle Fibres for Applications in Computational Skeletal Muscle Mechanics, Springer, New York, 2011.
[13] W. Z, A semi-automatic method for robust and efficient identification of neighboring muscle cells, Pattern Recogn. 53 (2015) 300–312 (Volume 53, May 2016, Pages 300-312).
[14] Z. Wang, H. Li, Generalizing cell segmentation and quantification, BMC Bioinf. 18 (1) (2017) 189.
[15] J. Pingel, et al., Injection of high dose botulinum-toxin A leads to impaired skeletal muscle function and damage of the fibrilar and non-fibrilar structures, Sci. Rep. 7 (1) (2017) 14746.
[16] B. Zeller-Plumhoff, et al., Investigation of microvascular morphological measures for skeletal muscle tissue oxygenation by image-based modelling in three dimensions, J. R. Soc. Interface 14 (135) (2017).
[17] B. Zeller-Plumhoff, et al., Phase contrast synchrotron radiation computed tomography of muscle spindles in the mouse soleus muscle, J. Anat. 230 (6) (2017) 859–865.
[18] M.S. Milenkovic, S.K. Dragos S, Skeletal Muscle; from Pharmacology to Clinical Practice; The Modern Approach to the Histopathological Diagnosis of Muscle Disease, (2015), pp. 155–170.
[19] T.B. Dyrby, et al., Validation strategies for the interpretation of microstructure imaging using diffusion MRI, Neuroimage 182 (2018) 62–79.
[20] Y. Hwu, G. Margaritondo, A.S. Chiang, Q&A: why use synchrotron x-ray tomography for multi-scale connectome mapping? BMC Biol. 15 (1) (2017) 122.
[21] Y.T.W. Hwu, A. Groso, G. Margaritondo, H.J. Je, Coherence-enhanced synchrotron radiology: simple theory and practical applications, J. Phys. Appl. Phys. 35 (13) (2002).
[22] P.C.J. Buseck, L. Eyring, High-Resolution Transmission Electron Microscopy - and Associated Techniques, Oxford University Press, 1989 ISBN: 9780195042757.
[23] M.W.A. Kass, D. Terzopoulos, Snakes: active counter models, Int. J. Comput. Vis. 1 (321) (1988).
[24] K. Li, et al., Optimal surface segmentation in volumetric images–a graph-theoretic approach, IEEE Trans. Pattern Anal. Mach. Intell. 28 (1) (2006) 119–134.
[25] J.G.G. Bigun, Optimal Orientation Detection of Linear Symmetry, Thesis report, Linkoping studies in science and technology (1986), p. 85.
[26] S. J, Estimating the Continuous Entropy of a Discrete Set of Orientations in R^3 Technical Report 2018/1, Department of Computer Science, University of Copenhagen, 2018.
[27] R. Malaiya, et al., The morphology of the medial gastrocnemius in typically developing children and children with spastic hemiplegic cerebral palsy, J. Electromyogr. Kinesiol. 17 (6) (2007) 657–663.
[28] S.J. Obst, et al., Quantitative 3-D ultrasound of the medial gastrocnemius muscle in children with unilateral spastic cerebral palsy, Ultrasound Med. Biol. 43 (12) (2017) 2814–2823.
[29] K. Ohata, et al., Measurement of muscle thickness as quantitative muscle evaluation for adults with severe cerebral palsy, Phys. Ther. 86 (9) (2006) 1231–1239.
[30] A. Shkedy Rabani, et al., Duration and patterns of habitual physical activity in adolescents and young adults with cerebral palsy, Dev. Med. Child Neurol. 56 (7) (2014) 673–680.
[31] S.L. Carlon, et al., Differences in habitual physical activity levels of young people with cerebral palsy and their typically developing peers: a systematic review, Disabil. Rehabil. 35 (8) (2013) 647–655.
[32] D.B. Maltais, et al., Factors related to physical activity in adults with cerebral palsy may differ for walkers and nonwalkers, Am. J. Phys. Med. Rehabil. 89 (7) (2010) 584–597.
[33] L.E. Mitchell, J. Ziviani, R.N. Boyd, Characteristics associated with physical activity among independently ambulant children and adolescents with unilateral cerebral palsy, Dev. Med. Child Neurol. 57 (2) (2015) 167–174.
[34] M. Gough, A.P. Shortland, Could muscle deformity in children with spastic cerebral palsy be related to an impairment of muscle growth and altered adaptation? Dev. Med. Child Neurol. 54 (6) (2012) 495–499.
[35] M. Willerslev-Olsen, et al., Impaired muscle growth precedes development of increased stiffness of the triceps surae musculotendinous unit in children with cerebral palsy, Dev. Med. Child Neurol. 60 (7) (2018) 672–679.